

Spontaneous magnetic skyrmions in single-layer CrInX_3 ($\text{X}=\text{Te}, \text{Se}$)

Wenhui Du, Kaiying Dou, Zhonglin He, Ying Dai*, Baibiao Huang, Yandong Ma*

School of Physics, State Key Laboratory of Crystal Materials, Shandong University, Shandan Street 27, Jinan 250100, China

*Corresponding author: daiy60@sina.com (Y.D.); yandong.ma@sdu.edu.cn (Y.M.)

Abstract

The realization of magnetic skyrmions in nanostructures holds great promise for both fundamental research and device applications. Despite recent progress, intrinsic magnetic skyrmions in two-dimensional lattice are still rarely explored. Here, using first-principles calculations and Monte-Carlo simulations, we report the identification of spontaneous magnetic skyrmions in single-layer CrInX_3 ($\text{X}=\text{Te}, \text{Se}$). Due to the joint effect of broken inversion symmetry and strong spin-orbit coupling, inherent large Dzyaloshinskii–Moriya interaction occurs in both systems, endowing the intriguing Néel-type skyrmions in the absence of magnetic field. By further imposing moderate magnetic field, the skyrmion phase can be obtained and is stable within a wide temperature range. Particularly for single-layer CrInTe_3 , the size of skyrmions is sub-10 nm and the skyrmion phase can be maintained at an elevated temperature of ~ 180 K. In addition, the phase diagrams of their topological spin textures under the variation of magnetic parameters of D , J , and K are mapped out. Our results greatly enrich the research of 2D skyrmionics physics.

Introduction

Magnetic skyrmion, a whirling spin texture, has been attracting extensive attention in recent research since it is important for fundamental physics and anticipated to be the next generation of information carriers [1-7]. Each magnetic skyrmion is characterized by a topological invariant called the topological charge Q , which is an integer that cannot be changed by a continuous transformation of magnetism. Because of such a topological nature, magnetic skyrmions are rather robust against environmental disturbance [8,9]. This combined with their small size and efficient current-driven dynamics render magnetic skyrmions promising for novel device applications, such as racetrack memory devices and neuromorphic computing devices [10-12]. Magnetic skyrmions are first experimentally verified in cubic B20 MnSi [13,14] and subsequently in epitaxial magnetic thin films such as Fe/Ir(111) [15] and Ir/Co/Pt [16]. Though highly valuable, such systems suffer from extremely narrow temperature region as well as harsh fabrication technology, limiting their practical application as well as integration [14-18].

Recently, long-range magnetism is discovered in two-dimensional (2D) materials [19-23]. This provides a promising alternative avenue for exploring exotic topologically nontrivial spin phenomena. The physics of magnetic skyrmions usually correlate to the competition between Dzyaloshinskii–Moriya interaction (DMI) and exchange coupling or magnetic anisotropy. Note that most 2D magnetic materials exhibit inversion symmetry, the existence of the essential DMI is excluded in them. There are several strategies to break the inversion symmetry of 2D lattice, such as electric field [24], proximity effect [25,26], and Janus structure [27-32]. Particularly, Janus structure with intrinsic inversion symmetry breaking has been predicted to be a promising way for establishing significant DMI [33,34]. As Janus MoSSe has been already grown employing different methods [35,36], Janus materials also show high experimental feasibility. Nevertheless, such 2D Janus materials exhibiting magnetic skyrmionics states are rather scarce, and up to now, only a few candidates have been reported [27-32].

Here, via first-principles calculations and Monte-Carlo simulations, we unveil that Janus single-layer (SL) CrInX_3 ($X=\text{Te, Se}$), derived from the prototype In_2X_3 , are promising 2D ferromagnetic semiconductors with skyrmionics physics. Both systems present inherent large DMI, which is originated from the combined effect of broken inversion symmetry and strong spin-orbit coupling (SOC). This yields the intriguing Néel-type skyrmions in both systems in the absence of magnetic field. Upon applying moderate magnetic field, the skyrmion phase can be realized, which is revealed to be robust within a rather wide temperature range. Especially for single-layer CrInTe_3 , the nontrivial spin texture is sub-10 nm and skyrmion phase can be preserved at an elevated temperature of up to ~ 180 K, which are technologically desirable. Furthermore, the dependence of their topological spin textures on D , J , and K are systematically discussed. These results demonstrated that SL CrInX_3

can be excellent candidates for skyrmionics applications.

Methods

First-principles calculations are performed based on density functional theory (DFT) as implemented in Vienna ab initio simulation package (VASP) [37,38]. The generalized gradient approximation (GGA) in form of Perdew-Burke-Ernzerhof (PBE) functional is used to treat the electron exchange-correlation interactions [39]. The plan-wave cutoff energy is set to 520 eV. The convergence criterion for force and energy are set to 0.01 eV/Å and 1×10^{-6} eV, respectively. The vacuum space along z direction is set to 25 Å. The Monkhorst-Pack k-point mesh of $15 \times 15 \times 1$ is adopted to sample the 2D Brillouin zone. $16 \times 4 \times 1$ k-point mesh is adopted for 1×4 supercell to calculate DMI parameters. To describe well the strong correlations of 3d electrons, GGA +U method is adopted with effective Hubbard $U = 3$ eV for 3d electrons of Cr atom, as employed in previous works [24,40]. Phonon spectra is obtained by PHONOPY code based on $3 \times 3 \times 1$ supercell [41]. Ab initio molecular dynamics (AIMD) simulations are performed at 300 K for 5 ps with a time step of 1 fs using $4 \times 4 \times 1$ supercell [42].

Parallel tempering Monte-Carlo (MC) simulations [43] with the Metropolis algorithm are carried out using the Hamiltonian of Eq. (3) presented below. All MC simulations are gradually cooled down from an initial disordered state at high temperature (660 K + investigated low temperature) to the investigated low temperature. For each simulated temperature, we used 10^5 MC steps for thermalization. To obtain the low-energy spin textures of SL CnInX_3 , the $320 \times 320 \times 1$ supercell with periodic boundary conditions is adopted.

For the convenience of discrete lattice, the topological charge Q is calculated based the method proposed by Berg and Lüscher and following the expression [44]

$$Q = \frac{1}{4\pi} \sum_l qn \quad (1)$$

$$\tan \frac{qn}{2} = \frac{\mathbf{s}_i^n \cdot (\mathbf{s}_j^n \times \mathbf{s}_k^n)}{1 + \mathbf{s}_i^n \cdot \mathbf{s}_j^n + \mathbf{s}_j^n \cdot \mathbf{s}_k^n + \mathbf{s}_k^n \cdot \mathbf{s}_i^n} \quad (2)$$

Here, \mathbf{s}_i^n , \mathbf{s}_j^n , \mathbf{s}_k^n are the three spin vectors of the n^{th} equilateral triangle in the anticlockwise lattice.

Results and Discussion

Figs. 1(a,b) display the crystal structure of Janus SL CrInX_3 . It presents the space group of $P3m1(C_{3v})$, and consists five atomic layers stacked in the sequence of X-In-X-Cr-X. Each Cr atom coordinated with six X atoms, forming a distorted octahedral geometry ($l_1 \neq l_2$). Obviously, the inversion symmetry of SL CrInX_3 is broken. The lattice constants of SL CrInX_3 are listed in **Table S1**. To determine the bonding nature in SL CrInX_3 , we calculate the electron localized function (ELF). As shown in **Fig. 1(c)** and **Fig. S1**, In-X bond exhibits a covalent character, while Cr-X bond shows an

ionic feature. To assess the stability of SL CrInX₃, we first calculate its phonon spectra. As shown in **Fig. S2**, there is only a tiny imaginary frequency around the Γ point, indicating its dynamic stability. Its thermal stability is further investigated by performing AIMD simulations. The slight free-energy fluctuation and well-defined structures confirm the thermal stability of SL CrInX₃, see **Fig. S3**.

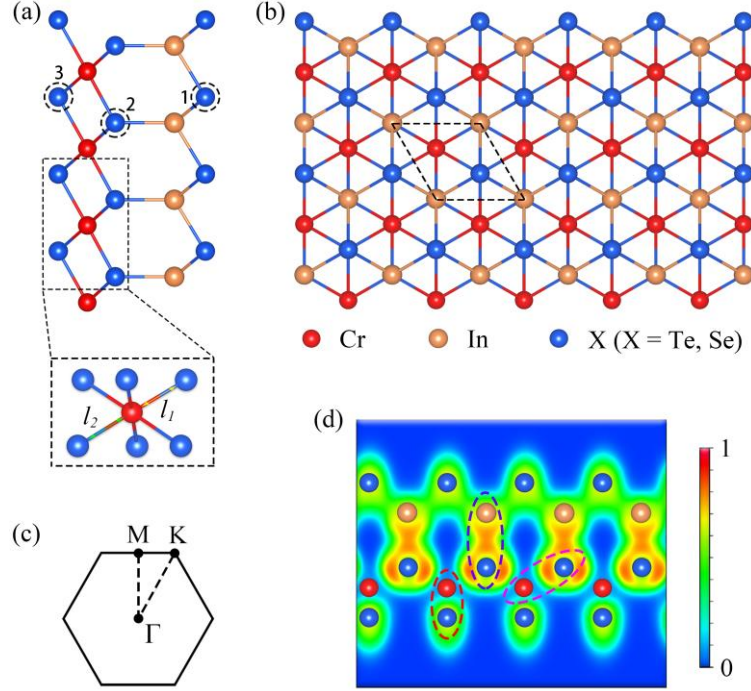


FIG. 1. (a) Crystal structure of SL CrInX₃ from (a) side and (b) top views. Inset in (a) shows the coordinate environment of Cr atom. In (b), the unit cell is represented by the black dotted lines. (c) 2D Brillouin zone. (d) Map of electron localization function (ELF) of SL CrInTe₃, where 0 and 1 indicate vanished and accumulated electron densities, respectively.

Concerning Cr atom, its valence electronic configuration is 3d⁴4s². In SL CrInX₃, each Cr atom donates three electrons to the six coordinated X atoms, resulting in the valence electronic configuration of 3d³4s⁰. Under the distorted octahedral crystal field, Cr-3d orbitals split into two groups: higher-lying e_g ($d_{xy}, d_{x^2-y^2}$) and lower-lying t_{2g} (d_{xz}, d_{yz}, d_{z^2}). The three left electrons of Cr atom would half-occupy t_{2g} orbitals, yielding a magnetic moment of 3 μ_B on each Cr atom. As shown in **Fig. 2(a)**, the magnetic moment is mainly distributed on the Cr atoms.

To investigate the interactions of magnetic moments in SL CrInX₃, we adopt a Heisenberg spin Hamiltonian:

$$H = -J \sum_{\langle i,j \rangle} \mathbf{S}_i \cdot \mathbf{S}_j - \lambda \sum_{\langle i,j \rangle} S_i^z S_j^z - K \sum_i (S_i^z)^2 - \sum_{\langle i,j \rangle} \mathbf{D}_{ij} \cdot (\mathbf{S}_i \times \mathbf{S}_j) - mB \sum_i S_i^z \quad (3)$$

Here, \mathbf{S}_i is the unit vector of Cr atom at site i . $\langle i,j \rangle$ represents the nearest-neighbor sites. J , λ , K

and D_{ij} represent the parameters of Heisenberg isotropic exchange, anisotropic symmetric exchange, single ion anisotropy and DMI, respectively. The last term is Zeeman energy, where m and B stand for the on-site magnetic moment of Cr atom and the external magnetic field, respectively. The magnetic parameters of J , λ , and K are obtained by considering four different magnetic configurations, see **Fig. S4**. As listed in **Table S1**, J are calculated to be 26.47 and 26.36 meV, respectively, for SL CrInSe₃ and CrInTe₃. The positive values indicate that the magnetic interactions in both systems prefer ferromagnetic (FM) coupling. Such FM coupling is related to their structures, namely, the Cr-X-Cr bonding angle is close to 90° for both systems, wherein FM super-exchange would dominate the magnetic exchange interaction according to the Goodenough-Kanamori-Anderson rules [45,46]. **Figs. S5** displays the band structures of SL CrInSe₃ and CrInTe₃, which are semiconductors with an indirect bandgap of 1.05 and 0.25 eV, respectively. Therefore, both systems are 2D FM semiconductors.

For establishing long-range FM coupling, magnetic anisotropy is essential. As listed in **Table S1**, SL CrInTe₃ exhibits $K = 1.544$ meV and $\lambda = 0.1003$ meV, suggesting large out-of-plane magnetic anisotropy. Different from SL CrInTe₃, SL CrInSe₃ shows $K = 0.262$ meV and $\lambda = -0.0063$ meV, indicating that its single ion anisotropy and anisotropic symmetric exchange prefer in-plane and out-of-plane magnetizations, respectively. Given the fact that K is two orders of magnitude larger than λ , SL CrInSe₃ also favors out-of-plane magnetization. It is interesting to note that although the λ and K parameters in these two systems are significantly different, their J parameters are roughly identical, as shown in **Fig. 2(b)**. This discrepancy is sought into the difference in SOC strength, which is proportional to Z^4 (Z is the atomic number). Compared with Se atom, Te atom is heavier, so the SOC effect in CrInTe₃ is stronger, resulting in more significant anisotropic symmetric exchange λ and single ion anisotropy K . In contrast, for Heisenberg isotropic exchange J , it is less affected by SOC. Based on the magnetic parameters of J , λ , and K , the Curie temperature T_c of SL CrInTe₃ and CrInSe₃ is estimated to be 340 K and 295 K, respectively, which is dramatically larger than that of CrI₃ (45 K) [19] and bilayer Cr₂Ge₂Te₆ (28 K) [21].

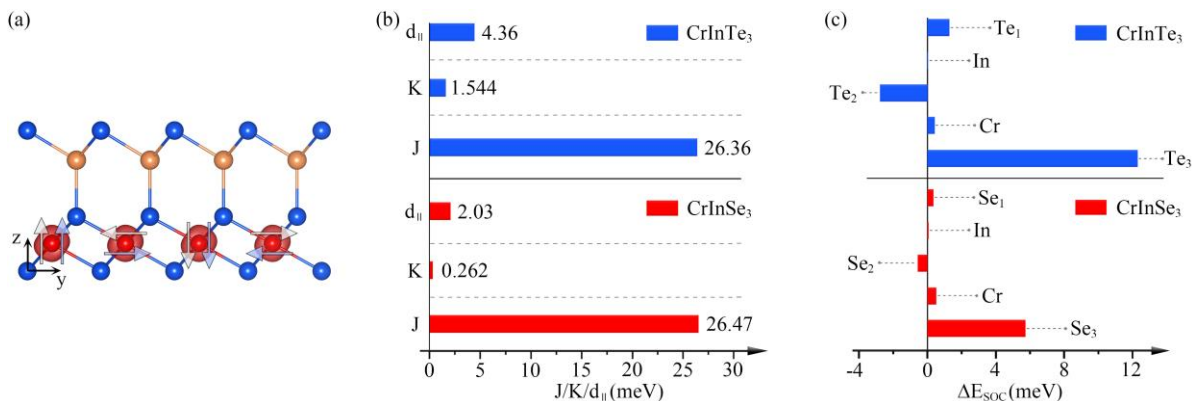


FIG. 2. (a) Spin charge density of SL CrInTe₃. White/blue vectors in (a) indicate the left/right-hand spin-spiral configurations used to obtain the in-plane DMI parameters d_{\parallel} and atomic projected SOC energy. (b) Isotropic exchange coupling parameter J , single ion anisotropy parameter K and in-plane DMI parameter d_{\parallel} of SL CrInX₃. (c) SOC energy projected on atoms (ΔE_{soc}) for SL CrInX₃.

We then consider the left- and right-hand spin-spiral configurations [Fig. 2(a)] to obtain the DMI parameters \mathbf{D}_{ij} . According to Moriya's rule [34], because the mirror plane passes through the middle of the bond between two adjacent Cr atoms, the DMI vector \mathbf{D}_{ij} for the nearest-neighbor Cr atoms is perpendicular to their bond. \mathbf{D}_{ij} can be written as $\mathbf{D}_{ij} = d_{\parallel}(\mathbf{z} \times \mathbf{u}_{ij}) + d_{\perp}\mathbf{z}$, where \mathbf{z} and \mathbf{u}_{ij} represent the unit vectors pointing along the z direction and from site i to site j , respectively. Since the out-of-plane component of \mathbf{D}_{ij} plays a negligible role in the formation of skyrmions, we only focus on its in-plane component d_{\parallel} . Remarkably, d_{\parallel} in SL CrInTe₃ (CrInSe₃) is rather large, which is calculated to be 4.36 (2.03) meV. Especially for SL CrInTe₃, d_{\parallel} is much larger than the values reported in most previous studies [15,29-32,47]. More importantly, the d_{\parallel}/J ratio is found to be 0.165 (0.077) for SL CrInTe₃ (CrInSe₃), which is within (near) the typical range of 0.1- 0.2 for more likely forming magnetic skyrmions [48].

To get further insight into the DMI in SL CrInX₃, we project the associated SOC energy ΔE_{soc} [ΔE_{soc} is defined as the energy difference between left- and right-hand spin-spiral configurations] on each atom. As shown in Fig. 2(c), the main DMI contribution does not originate from the magnetic Cr atoms, but from its adjacent X atoms. In this case, the X atoms, serving as effective sites of SOC, introduce the spin-orbit scattering necessary for DMI. This clearly indicates that the Fert-Levy mechanism [49,50] is responsible for DMI in SL CrInX₃. As larger Z corresponds to stronger SOC, more significant DMI is obtained in SL CrInTe₃. In addition, we find that $|\Delta E_{\text{soc}}|$ from X₃ atom is much larger than that from X₂ atom. This correlates to the strong covalent bonding between X₂ and In atoms, which weakens the coupling between X₂ and Cr atoms and thus results in a relatively small DMI contribution from X₂ atom.

Based on the first-principles parametrized Hamiltonian of Eq. (3), parallel tempering MC simulations are performed to explore the possible topological spin textures in SL CrInX₃. The topological stability of magnetic skyrmions is characterized by topological charge Q , which is defined as $Q = \frac{1}{4\pi} \int \mathbf{m} \cdot \left(\frac{\partial \mathbf{m}}{\partial x} \times \frac{\partial \mathbf{m}}{\partial y} \right) dx dy$ [9,44]. Here, \mathbf{m} is the normalized magnetization vector. Figs. 3(a,b) present the spin textures of SL CrInX₃. Without applying magnetic field, labyrinth domains are observed in both systems at 0 K. Aside from labyrinth domains, intriguingly, the Néel-

type magnetic skyrmions with $Q = \pm 1$ also exist in both systems spontaneously. Such a mixed phase is referred to as spin spiral phase (SS) below. It is worthy emphasizing that for SL CrInTe₃, the magnetic skyrmions occur in different domains, which presents opposite polarization and thus opposite topological charge Q ; see **Fig. 3(b)**. Moreover, the diameter of magnetic skyrmions in CrInTe₃ is about 7.6 nm, significantly smaller than those of MnSTe (40 nm) [28], LaCl/In₂Se₃ (23 nm) [25] and Cr(I, Cl)₃ (10.5 nm) [29]. Such a small size within sub-10nm is technologically desired for future skyrmionics devices. Different from the case of CrInTe₃, the magnetic skyrmions in SL CrInSe₃ occur in one domain, and its size is about 27.8 nm.

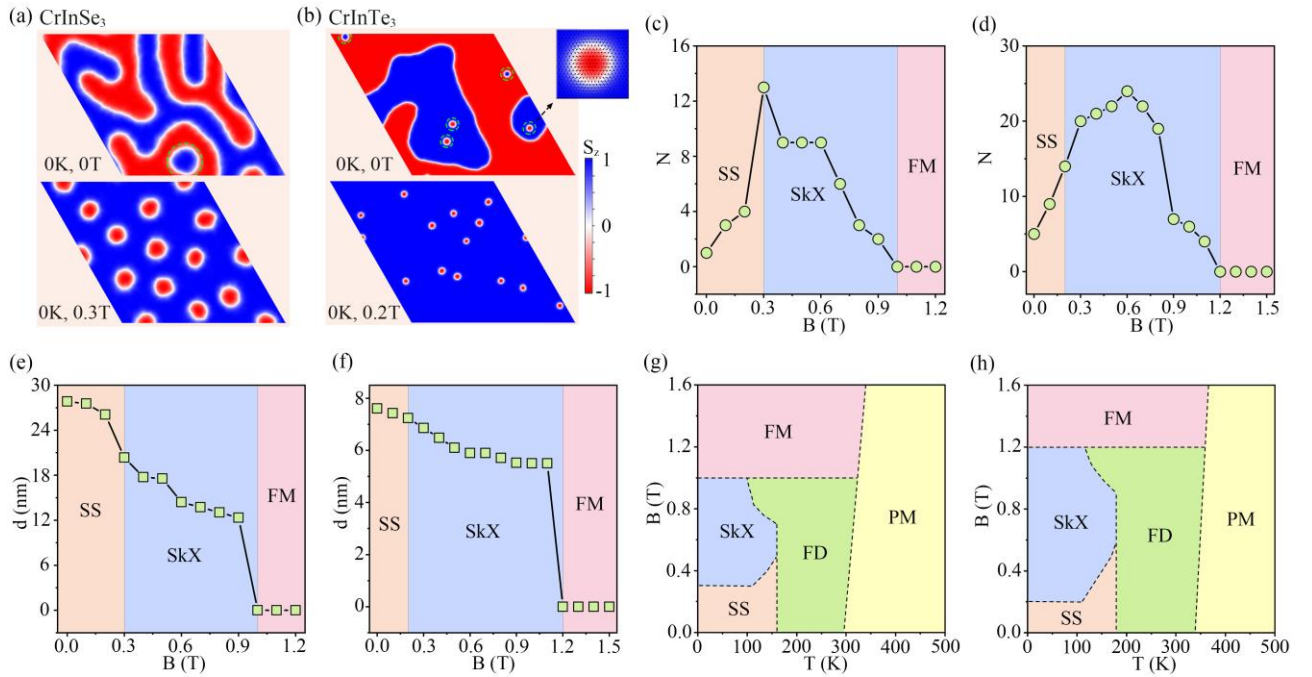


FIG. 3. Spin textures of SL (a) CrInSe₃ and (b) CrInTe₃ without and with applying magnetic field (B) at 0 K. Inset in (b) shows the magnetization distribution in skyrmion. Colors are assigned for out-of-plane magnetization components and black arrows represent the in-plane components. Number (N) of skyrmions for SL (c) CrInSe₃ and (d) CrInTe₃ as a function of B . Skyrmion diameters for SL (e) CrInSe₃ and (f) CrInTe₃ as a function of B . Magnetic phase diagrams for SL (g) CrInSe₃ and (h) CrInTe₃ with temperatures T and B . SkX, SS, FM in (b-h) and FD, PM in (g, h) indicate skyrmion, spin spiral, fluctuation-disorder, ferromagnetic and paramagnetic phases, respectively.

We then explore the effect of external magnetic field on the topological spin structures of SL CrInX₃. For SL CrInTe₃, the labyrinth domain shrinks with increasing magnetic field, and disappears completely at 0.2 T, see **Fig. 3(b)**. In this case, only isolated skyrmions are left in a FM background,

forming the magnetic skyrmion (SkX) phase. Importantly, as shown in **Fig. 3(d)**, this SkX phase can be preserved in a wide magnetic field range of 0.2 – 1.2 T. For the density of skyrmions, it increases with increasing the magnetic field from 0 T to 0.6 T. For the cases of 0.6 – 1.2 T, the density of skyrmions decreases significantly, and the skyrmions pattern is completely magnetized into the trivial FM phase at 1.2 T. **Fig. 3(f)** shows the impact of magnetic field on the skyrmion size for SL CrInTe₃, from which we can see that the skyrmion size decreases with increasing magnetic field. In detail, the skyrmion diameter reduces from about 7.6 nm at 0 T to 5.5 nm at 1.1 T and then shrinks into a FM background at 1.2 T. The underlying physics for this phenomenon is related to that fact that external magnetic field favors the out-of-plane magnetization as that of the FM background.

The roughly similar scenario is also observed in SL CrInSe₃. With increasing magnetic field, the spin structure of SL CrInSe₃ undergoes a SS-SkX-FM phase transition. All the labyrinth domains shrink at 0.3 T, leading to the skyrmion lattice, see **Fig. 3(a)**. By further increasing the magnetic field, the density of skyrmions decreases, and drops to zero at 1 T, which gives rise to a trivial FM phase. With respect to the case of SL CrInTe₃, the SkX phase of SL CrInSe₃ can be preserved in a relatively narrow magnetic field range of 0.3 – 1 T [**Fig. 3(c)**]. Moreover, the increase of magnetic field also results in the shrinking of skyrmion size before transforming into FM phase, i.e., the skyrmion size decreases from 27.8 nm at 0 T to 12.3 nm at 0.9 T, see **Fig. 3(e)**.

Considering that thermal fluctuations may destabilize magnetic order, we further study the temperature effect on topological spin structures in SL CrInX₃ under various magnetic fields. The corresponding magnetic phase diagrams for SL CrInX₃ are displayed in **Figs. 3(g,h)**. We can see that besides SS, SkX and FM phases, two new phases [i.e., fluctuation-disorder (FD) and paramagnetic (PM) phases] emerge. In FD phase, arising from thermal fluctuation, on one hand, the vortex of skyrmion is partially deformed, and on the other hand, the breaking of skyrmions increases the number of little vortices. The former and latter factors would decrease and increase topological charge Q . Here, we take $|Q - 1| > 0.01$ as the judgment standard for the transformation of SkX phase into FD phase. In PM phase, magnetic order is completely destroyed, and thus spin texture becomes disordered as well. The Curie temperature under different external magnetic fields is calculated to judge the critical temperature of phase transition into PM phase.

From **Fig. 3(h)**, we can see that SL CrInTe₃ is stabilized in SS phase at low temperature and low magnetic field ($B < 0.2$ T). With increasing temperature, the SS phase is transformed into FD and PM phases, successively. When external magnetic field approaches 0.2 T, the labyrinth domain

completely shrinks to isolated skyrmions at 0 K, suggesting the transition from SS to SkX phases. Under the magnetic field of 0.2 – 0.6 T, with rising temperature, the SkX phase is transformed into SS phase, then FD phase and finally PM phase. While under 0.6 – 1.2 T, with increasing temperature, the SkX phase is directly transformed into FD phase, and then PM phase. It is worth noting that when the magnetic field exceeds 0.9 T, the maximum temperature that the skyrmions can withstand gradually decreases. This suggests that moderate magnetic field can be used to establish skyrmions. Under magnetic field above 1.2 T, the SkX phase is magnetized into FM phase. This scenario is roughly shared by the case of SL CrInSe₃; see **Fig. 3(g)**. Therefore, by modulating external magnetic field and temperature, we can control the generation and annihilation of skyrmions, and thus the topological phase transition, in SL CrInX₃. We wish to point out that the skyrmions of SL CrInX₃ can be obtained in a considerable wide temperature range. Especially for SL CrInTe₃, the SkX phase can be preserved as temperatures rising up to ~180 K.

To deeply understand the skyrmionics physics in SL CrInX₃, taking SL CrInTe₃ as an example, we investigate the relationships between topological spin structures and magnetic parameters of D , J and K . Since D/J is regarded as an important parameter to estimate the existence of skyrmions, we first explore the dependence of spin texture on D/J under different external magnetic fields, while keeping other parameters the same as those in SL CrInTe₃ except λ . Considering λ in SL CrInX₃ is negligible, it is set to zero in the simulation for simple. As shown in **Fig. 4(a)**, the spin texture undergoes a FM-SkX-SS transition with increasing D/J under different external magnetic fields. In SkX region, the size and density of skyrmions increase with increasing D/J . In SS region, as the D/J increases, the density of labyrinth domains increases, while the size reduces. Moreover, as shown in **Fig. 4(a)**, when the magnetic field increases, the SkX phase moves to larger D/J region. This indicates that a larger external magnetic field is required for stabilizing the skyrmions in system with larger D/J .

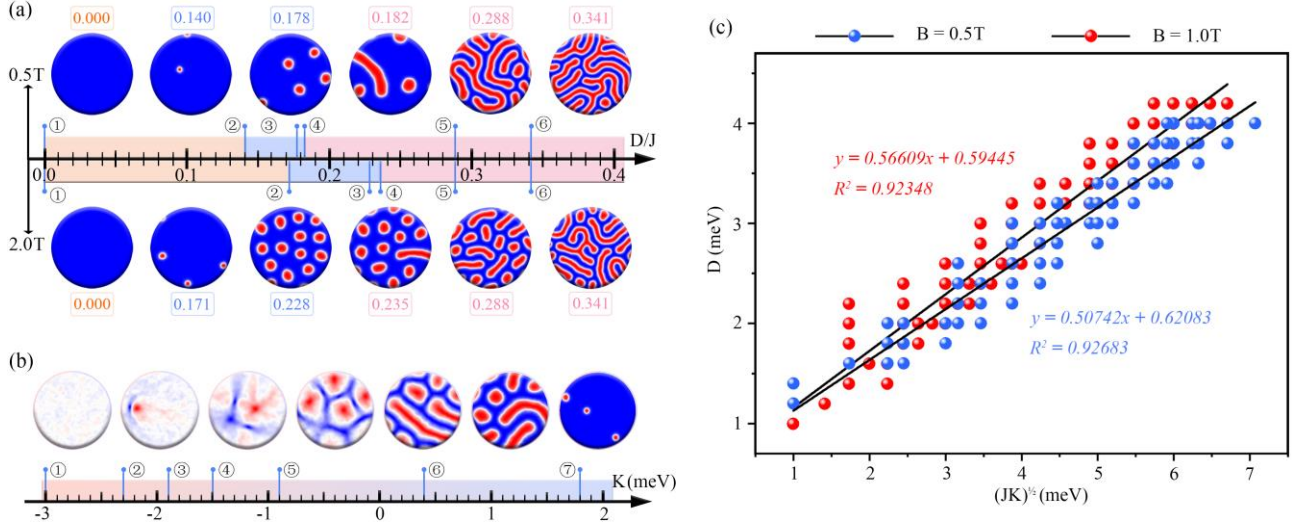


FIG. 4. (a) Evaluation of spin textures as a function of D/J under different external magnetic fields. (b) Evaluation of spin texture as a function of K under the external magnetic field of 0.5 T. (c) Linear scaling relation between D and \sqrt{JK} of SkX phase under different external magnetic fields.

The evaluation of spin textures as a function of D/J under different magnetic fields is related to the competition among D , J and external magnetic field B . Specifically, J and B tend to force the parallel arrangement of magnetic moments, while D induces the magnetic moments to be arranged noncollinearly. In the SkX region, when D/J is relatively small, the magnetic exchange coupling plays a more important role, which reduce the vortices in the FM background and make the magnetic moments' rotation from the $-z$ direction at the center of skyrmion to z direction at the boundary at a small atomic scale. In this case, the skyrmions with relatively small-size and low-density can be obtained. Upon decreasing D/J close to zero, DMI is negligible, and the strong magnetic exchange coupling J leads the parallel arrangement of magnetic moments, i.e., FM phase. On the other hand, when D/J is large enough, DMI plays a dominated role, benefiting for the emergence of labyrinth domains. With these results in hand, we can understand the evaluation of spin textures discussed above.

After establishing the roles of D and J , also taking SL CrInTe₃ as an example, we next study the effect of K on the topological spin texture. As shown in **Fig. 4(b)**, with increasing K from -3 to 2 meV, the spin texture undergoes an iFM (in-plane FM)-bimeron-SS-SkX phase transition. Moreover, we find that the size of topological spin textures decreases with increasing $|K|$. When K is positive, the perpendicular magnetic anisotropy provides the energy gain to sustain an out-of-plane spin alignment, thus promoting the formation of Néel-type skyrmions. For $K < 0$, the system favors in-

plane spin alignment, converting the Néel-type skyrmions into bimerons. Furthermore, similar to J , K is prone to force the magnetic moment in a parallel arrangement. In this regard, a large $|K|$ can suppress the modulated labyrinth domains and skyrmions, and the reduction of the size of skyrmions or bimerons.

From above, we can see that D , J and K can significantly affect the formation and characters of SkX phase. To help the rational design of SkX phases, it is important to identify a universal descriptor based on these three magnetic parameters. To this end, we conduct high throughput calculations with changing each magnetic parameter independently under different magnetic fields. As shown in **Fig. 4(c)**, intriguingly, relationships between D and \sqrt{JK} of SkX phase are linear under different magnetic fields, and a stronger magnetic field corresponds to a larger slope. This suggests that D/\sqrt{JK} can be used to estimate the required external magnetic field for forming SkX phase.

Conclusion

To summarize, we propose that SL CrInX₃ are compelling 2D ferromagnetic semiconductors with skyrmionics physics on the basis of first-principles calculations and Monte-Carlo simulations. We find that, due to the inherent large DMI, both systems exhibit Néel-type skyrmions, without needing the external magnetic field. Moreover, the skyrmion phase can be established in both systems under a moderate magnetic field, and such phase is stable within a rather wide temperature range. In particular for SL CrInTe₃, the skyrmion size is sub-10 nm, and SkX phase can be preserved at an elevated temperature of up to ~180 K. In addition, we also systematically investigate the dependence of the topological spin textures on D , J , and K , and reveal that D/\sqrt{JK} can be used to estimate the required magnetic field for forming SkX phase.

Acknowledgement

This work is supported by the National Natural Science Foundation of China (No. 12074217), Shandong Provincial Natural Science Foundation (Nos. ZR2019QA011 and ZR2019MEM013), Shandong Provincial Key Research and Development Program (Major Scientific and Technological Innovation Project) (No. 2019JZZY010302), Shandong Provincial Key Research and Development Program (No. 2019RKE27004), Shandong Provincial Science Foundation for Excellent Young Scholars (No. ZR2020YQ04), Qilu Young Scholar Program of Shandong University, and Taishan Scholar Program of Shandong Province.

Competing interests

The authors declare no competing interests.

Date availability

The authors declare that the data supporting the findings of this study are available within the paper and its supplementary information files.

References

- [1] U. K. Roessler, A. Bogdanov and C. Pfleiderer, Spontaneous skyrmion ground states in magnetic metals. *Nature* **2006**, 442, 797-801.
- [2] X. Z. Yu, Y. Onose, N. Kanazawa, J. H. Park, J. H. Han, Y. Matsui, N. Nagaosa and Y. Tokura, Real-space observation of a two-dimensional skyrmion crystal. *Nature* **2010**, 465, 901-904.
- [3] X. Z. Yu, Y. Onose, K. Kimoto, W. Z. Zhang, S. Ishiwata, Y. Matsui and Y. Tokura, Near room-temperature formation of a skyrmion crystal in thin-films of the helimagnet FeGe. *Nat. Mater.* **2011**, 10, 106-109.
- [4] J. Sampaio, V. Cros, S. Rohart, A. Thiaville and A. Fert, Nucleation, stability and current-induced motion of isolated magnetic skyrmions in nanostructures. *Nat. Nanotechnol.* **2013**, 8, 839-844.
- [5] O. Boulle, J. Vogel, H. Yang, S. Pizzini, D. de Souza Chaves, A. Locatelli, T. Menteş, A. Sala, L. Buda-Prejbeanu, O. Klein, M. Belmeguenai, Y. Roussigné, A. Stashkevich, S. Chérif, L. Aballe, M. Foerster, M. Chshiev, S. Auffret, I. Miron and G. Gaudin, Room-temperature chiral magnetic skyrmions in ultrathin magnetic nanostructures. *Nat. Nanotechnol.* **2016**, 11, 449-454.
- [6] A. Soumyanarayanan, M. Raju, A. L. Gonzalez Oyarce, A. K. C. Tan, M.-Y. Im, A. P. Petrović, P. Ho, K. H. Khoo, M. Tran, C. K. Gan, F. Ernult and C. Panagopoulos, Tunable room-temperature magnetic skyrmions in Ir/Fe/Co/Pt multilayers. *Nat. Mater.* **2017**, 16, 898-904.
- [7] W. Jiang, G. Chen, K. Liu, J. Zang, S. G. E. te Velthuis and A. Hoffmann, Skyrmions in magnetic multilayers. *Phys. Rep.* **2017**, 704, 1-49.
- [8] Y. Tokura and N. Kanazawa, Magnetic skyrmion materials. *Chem. Rev.* **2021**, 121, 2857-2897.
- [9] N. Nagaosa and Y. Tokura, Topological properties and dynamics of magnetic skyrmions. *Nature Nanotechnol.* **2013**, 8, 899-911.
- [10] A. Fert, V. Cros and J. Sampaio, Skyrmions on the track. *Nat. Nanotechnol.* **2013**, 8, 152.
- [11] W. Kang, Y. Huang, C. Zheng, W. Lv, N. Lei, Y. Zhang, X. Zhang, Y. Zhou and W. Zhao, Voltage controlled magnetic skyrmion motion for racetrack memory. *Sci. Rep.* **2016**, 6, 23164.
- [12] S. Li, W. Kang, X. Zhang, T. Nie, Y. Zhou, K. L. Wang and W. Zhao, Magnetic skyrmions for unconventional computing. *Mater. Horiz.* **2021**, 8, 854.
- [13] S. Mühlbauer, F. Jonietz, C. Pfleiderer, A. Rosch, A. Neubauer, R. Georgii and P. Böni, Skyrmion lattice in a chiral magnet. *Science* **2009**, 323 (5916), 915-919.
- [14] S. Mühlbauer, B. Binz, F. Jonietz, C. Pfleiderer, A. Rosch, A. Neubauer, R. Georgii and P. Böni, Skyrmion Lattice in a Chiral Magnet. *Science* **2019**, 323, 915.
- [15] S. Heinze, K. von Bergmann, M. Menzel, J. Brede, A. Kubetzka, R. Wiesendanger, G. Bihlmayer and S. Blügel, Spontaneous atomic-scale magnetic skyrmion lattice in two dimensions. *Nat. Phys.* **2011**, 7, 713-718.

- [16] C. Moreau-Luchaire, C. Moutafis, N. Reyren, J. Sampaio, C. A. F. Vaz, N. Van Horne, K. Bouzehouane, K. Garcia, C. Deranlot, P. Warnicke, P. Wohlhüter, J.-M. George, M. Weigand, J. Raabe, V. Cros and A. Fert, Additive interfacial chiral interaction in multilayers for stabilization of small individual skyrmions at room temperature. *Nat. Nanotechnol.* **2016**, 11, 444-448.
- [17] I. Kézsmárki, S. Bordács, P. Milde, E. Neuber, L. M. Eng, J. S. White, H. M. Rønnow, C. D. Dewhurst, M. Mochizuki, K. Yanai, H. Nakamura, D. Ehlers, V. Tsurkan and A. Loidl, Néel-type skyrmion lattice with confined orientation in the polar magnetic semiconductor GaV₄S₈. *Nature Mater* **2015**, 14, 1116-1122.
- [18] N. Romming, C. Hanneken, M. Menzel, J. E. Bickel, B. Wolter, K. von Bergmann, A. Kubetzka and R. Wiesendanger, Writing and Deleting Single Magnetic Skyrmions. *Science* **2013**, 341, 636-639.
- [19] B. Huang, G. Clark, E. Navarro-Moratalla, D. Klein, R. Cheng, K. Seyler, D. Zhong, E. Schmidgall, M. McGuire, D. Cobden, W. Yao, D. Xiao, P. Jarillo-Herrero and X. Xu, Layer-dependent ferromagnetism in a van der Waals crystal down to the monolayer limit. *Nature* **2017**, 546, 270-273.
- [20] Y. Deng, Y. Yu, Y. Song, J. Zhang, N. Z. Wang, Z. Sun, Y. Yi, Y. Z. Wu, S. Wu, J. Zhu, J. Wang, X. H. Chen and Y. Zhang, Gate-tunable room-temperature ferromagnetism in two-dimensional Fe₃GeTe₂. *Nature* **2018**, 563, 94-99.
- [21] C. Gong, L. Li, Z. Li, H. Ji, A. Stern, Y. Xia, T. Cao, W. Bao, C. Wang, Y. Wang, Z. Q. Qiu, R. J. Cava, S. G. Louie, J. Xia and X. Zhang, Discovery of intrinsic ferromagnetism in two-dimensional van der Waals crystals. *Nature* **2017**, 546, 265-269.
- [22] D. J. O'Hara, T. Zhu, A. H. Trout, A. S. Ahmed, Y. K. Luo, C. H. Lee, M. R. Brenner, S. Rajan, J. A. Gupta, D. W. McComb and R. K. Kawakami, Room Temperature Intrinsic Ferromagnetism in Epitaxial Manganese Selenide Films in the Monolayer Limit. *Nano Lett.* **2018**, 18, 3125-3131.
- [23] M. Bonilla, S. Kolekar, Y. Ma, H. C. Diaz, V. Kalappattil, R. Das, T. Eggers, H. R. Gutierrez, M.-H. Phan and M. Batzill, Strong room-temperature ferromagnetism in VSe₂ monolayers on van der Waals substrates. *Nat. Nanotechnol.* **2018**, 13, 289-293.
- [24] A. K. Behera, S. Chowdhury and S. R. Das, Magnetic skyrmions in atomic thin CrI₃ monolayer. *Appl. Phys. Lett.* **2019**, 114, 232402.
- [25] D. Chen, J. Wang and Z. Cheng, Controlling bimerons as skyrmion analogues by ferroelectric polarization in 2D van der Waals multiferroic heterostructures. *Nat Commun* **2020**, 11, 5930.
- [26] W. Sun, W. Wang, J. Zang, H. Li, G. Zhang, J. Wang and Z. Cheng, Manipulation of Magnetic Skyrmion in a 2D van der Waals Heterostructure via Both Electric and Magnetic Fields. *Adv. Funct. Mater.* **2021**, 31, 2104452
- [27] J. Liang, W. Wang, H. Du, A. Hallal, K. Garcia, M. Chshiev, A. Fert and H. Yang, Very large Dzyaloshinskii-Moriya interaction in two-dimensional Janus manganese dichalcogenides and its application to realize skyrmion states. *Phys. Rev. B* **2020**, 101, 184401.
- [28] J. Yuan, Y. Yang, Y. Cai, Y. Wu, Y. Chen, X. Yan and L. Shen, Intrinsic skyrmions in monolayer Janus magnets. *Phys. Rev. B* **2020**, 101, 094420.
- [29] C. Xu, J. Feng, S. Prokhorenko, Y. Nahas, H. Xiang and L. Bellaiche, Topological spin texture in Janus monolayers of the chromium trihalides Cr(I, X)₃. *Phys. Rev. B* **2020**, 101, 060404(R).
- [30] Y. Zhang, C. Xu, P. Chen, Y. Nahas, S. Prokhorenko and L. Bellaiche, Emergence of

- skyrmionium in a two-dimensional CrGe(Se,Te)₃ Janus monolayer. *Phys. Rev. B* **2020**, 102, 241107(R).
- [31] J. Jiang, X. Liu, R. Li and W. Mi, Topological spin textures in a two-dimensional MnBi₂(Se, Te)₄ Janus material. *Appl. Phys. Lett.* **2021**, 119, 072401.
- [32] Q. Cui, J. Liang, Z. Shao, P. Cui and H. Yang, Strain-tunable ferromagnetism and chiral spin textures in two-dimensional Janus chromium dichalcogenides. *Phys. Rev. B* **2020**, 102, 094425.
- [33] I. Dzyaloshinsky, A thermodynamic theory of “weak” ferromagnetism of antiferromagnetics. *J. Phys. Chem. Solids* **1958**, 4, 241.
- [34] T. Moriya, Anisotropic Superexchange Interaction and Weak Ferromagnetism. *Phys. Rev.* **1960**, 120, 91.
- [35] A.-Y. Lu, H. Zhu, J. Xiao, C.-P. Chuu, Y. Han, M.-H. Chiu, C.-C. Cheng, C.-W. Yang, K.-H. Wei, Y. Yang, Y. Wang, D. Sokaras, D. Nordlund, P. Yang, D. A. Muller, M.-Y. Chou, X. Zhang and L.-J. Li, Janus monolayers of transition metal dichalcogenides. *Nat. Nanotechnol.* **2017**, 12, 744.
- [36] J. Zhang, S. Jia, I. Kholmanov, L. Dong, D. Er, W. Chen, H. Guo, Z. Jin, V. B. Shenoy, L. Shi and J. Lou, Janus Monolayer Transition-Metal Dichalcogenides. *ACS Nano* **2017**, 11, 8192.
- [37] W. Kohn and L. J. Sham, Self-consistent equations including exchange and correlation effects, *Phys. Rev.* **1965**, 140, A1133.
- [38] G. Kresse and J. Furthmüller, Efficient iterative schemes for ab initio total-energy calculations using a plane-wave basis set, *Phys. Rev. B* **1996**, 54, 11169.
- [39] J. P. Perdew, K. Burke, and M. Ernzerhof, Generalized gradient approximation made simple, *Phys. Rev. Lett.* **1996**, 77, 3865.
- [40] G. Song, D. Li, H. Zhou, C. Zhang, Z. Li, G. Li, B. Zhang, X. Huang and B. Gao, Intrinsic room-temperature ferromagnetic semiconductor InCrTe₃ monolayers with large magnetic anisotropy and large piezoelectricity. *Appl. Phys. Lett.* **2021**, 118, 123102.
- [41] P. Giannozzi, S. Baroni, N. Bonini, M. Calandra, R. Car, C. Cavazzoni, D. Ceresoli, G. L. Chiarotti, M. Cococcioni, I. Dabo *et al.*, QUANTUM ESPRESSO: a modular and open-source software project for quantum simulations of materials. *J. Phys.: Condens. Matter* **2009**, 21, 395502.
- [42] H. J. Monkhorst and J. D. Pack, Special points for Brillouin-zone integrations. *Phys. Rev. B* **1976**, 13, 5188.
- [43] Y. Miyatake, M. Yamamoto, J. Kim, M. Toyonaga and O. Nagai, On the implementation of the 'heat bath' algorithms for Monte Carlo simulations of classical Heisenberg spin systems. *J. Phys. C: Solid State Phys.* **1986**, 19, 2539.
- [44] B. Berg and M. Lüscher, Definition and statistical distributions of a topological number in the lattice O(3) σ -model. *Nuclear Phys. B* **1981**, 190, 412-424.
- [45] J. B. Goodenough, Theory of the Role of Covalence in the Perovskite-Type Manganites [La, M(II)]MnO₃. *Phys. Rev.* **1955**, 100, 564-573.
- [46] J. Kanamori, Crystal Distortion in Magnetic Compounds. *J. Appl. Phys.* **1960**, 31, S14-S23.
- [47] C. Xu, P. Chen, H. Tan, Y. Yang, H. Xiang and L. Bellaiche, Electric-Field Switching of Magnetic

Topological Charge in Type-I Multiferroics. *Phys. Rev. Lett.* **2020**, 125, 037203.

[48] J. Kanamori, Crystal Distortion in Magnetic Compounds. *J. Appl. Phys.* **1960**, 31, S14–S23.

[49] A. Fert and P. M. Levy, Role of Anisotropic Exchange Interactions in Determining the Properties of Spin-Glasses. *Phys. Rev. Lett.* **1980**, 44, 1538.

[50] P. M. Levy and A. Fert, Anisotropy induced by nonmagnetic impurities in *Cu Mn* spin-glass alloys. *Phys. Rev. B* **1981**, 23, 4667.